Heliyon 10 (2024) e31702

Contents lists available at ScienceDirect

Heliyon

journal homepage: www.cell.com/heliyon

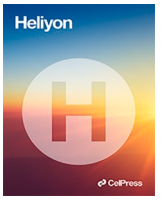

Research article

Metal-free adsorption and photodegradation methods for methylene blue dye removal using different reduction grades of graphene oxide

Sanju Mahich [a], Yogesh Kumar Saini [a], Vijay Devra [b], Kanika Aggarwal [c], Anuj Kumar [d], Dinesh Kumar [e], Amanpal Singh [a,**], Yogendra Arya [f,*]

[a] Department of Physics, University of Rajasthan, Jaipur, Rajasthan, 302004, India
[b] Janki Devi Bajaj Government Girls College, Kota, Rajasthan, 324001, India
[c] Department of Physics, Sant Longowal Institute of Engineering and Technology, Longowal, Punjab, 148106, India
[d] Department of Physics, J.C. Bose University of Science and Technology, YMCA, Faridabad, Haryana, 121006, India
[e] Gurugram University, Gurugram, Haryana, 122003, India
[f] Department of Electrical Engineering, J.C. Bose University of Science and Technology, YMCA, Faridabad, Haryana, 121006, India

ARTICLE INFO

Keywords:
Adsorption
Dye degradation
Graphene oxide
Photocatalytic activity

ABSTRACT

The release of organic pollutants and dyes into the environment by industries has had profound and harmful effects on both humans and ecosystems. Graphene oxide (GO) and its reduced form have been investigated for their effectiveness in removing pollutant dyes. GO nano-powder was synthesized using an improved version of Hummer's method and subsequently thermally reduced at various temperatures, including 125, 150, 175, and 200 °C, under vacuum conditions. In the X-ray diffraction spectra, an intense (001) diffraction peak was initially observed at 9.136° (2θ) for pristine GO. This peak gradually shifted towards higher angles as the reduction process took place and eventually disappeared when the GO was reduced at 200 °C. The intensity ratio of the D and G bands (ID/IG ratio) for GO nano-powder in the Raman spectra decreased from 0.94 to 0.76 due to the reduction process. The FTIR spectra of GO and reduced graphene oxide (rGO) also illustrated the reduction process. The bandgap of pristine GO significantly decreased from 2.31 to 0.73 eV, as determined by ultraviolet–visible (UV–Vis) diffuse reflectance spectrophotometry during the reduction process. The surface area and pore volume of both pristine GO and rGO-150 were determined using the BET (Brunauer-Emmett-Teller) and BJH (Barrett-Joyner-Halenda) methods. The results indicated an increase in the BET surface area from 6.61 to 7.86 m^2/g and a corresponding enhancement in pore volume from 0.118 to 0.128 cc/g after reduction. The adsorption and photocatalytic degradation behavior of pristine GO and reduced graphene oxides (rGOs) were examined using methylene blue dye. The pristine GO demonstrated impressive adsorption capability, effectively removing the dye by 85.78 % within just 15 min and achieving nearly 97 % removal after 4 h. In contrast, the highest photocatalytic degradation of methylene blue, about 47.58 %, was attained for the rGO sample reduced at 150 °C under the illumination of visible light.

* Corresponding author.
** Corresponding author.
E-mail addresses: amanbkn@gmail.com (A. Singh), mr.y.arya@gmail.com (Y. Arya).

https://doi.org/10.1016/j.heliyon.2024.e31702
Received 1 October 2023; Received in revised form 20 May 2024; Accepted 21 May 2024
Available online 23 May 2024

1. Introduction

Water is a critical element for all living creatures on Earth. In the recent years, water quality has deteriorated due to rapid industrialization, population growth, climate change, pesticides, and pollution [1]. According to the World Health Organization, waterborne diseases account for 4 billion cases of illness each year, resulting in more than 1.7 million deaths due to water pollution [2]. Consequently, water contamination and the scarcity of pure drinking water are major concerns worldwide.

The water is extensively used in the textile manufacturing industry for processes such as dyeing and washing materials. Synthetic dyes, which are harmful to ecosystems and humans, are present in wastewater from these treatments. The use of dyes in the textile industry continues to grow, with more than 20 % of dye effluents being discharged into water bodies, leading to health problems. These dyes are resistant to natural degradation due to their complex aromatic structure. As a result, various treatment methods have been employed to remove dyes, including ozonation, chlorination, photo-Fenton, electrochemical oxidation, advanced oxidation, reverse osmosis, photocatalysis, and adsorption [3–5]. Among these, adsorption is a simple, cost-effective, and promising technology for removing dye materials from wastewater, as inexpensive adsorbents with high adsorption capacity are readily available [6]. However, it has certain drawbacks such as the production of secondary waste, having limited capacity and requiring frequent replacement of the adsorbent material.

Photocatalysis is another popular method known for its simplicity. When incident light has energy equal to or greater than the band gap of the photocatalyst, electrons in the valence band become excited, generating electron-hole pairs. These electron-hole pairs then utilize water and surrounding oxygen molecules to produce reactive oxygen species (ROS) such as superoxide (O^{2-}) and hydroxyl (OH•) radicals, which are responsible for degrading dye molecules [1]. In both reactions, the surface area of the materials significantly influences dye removal [7].

Carbon-based materials are well-known for their high adsorption capacities due to electrostatic interactions with adsorbates and their porosity. Activated carbon is the most widely used adsorption material, but its large-scale production is costly, and in some cases, it exhibits limited adsorption properties [2]. Graphene Oxide (GO) has emerged as a potential material for dye adsorption applications. GO offers high mechanical strength, unique electronic properties, low density, high catalytic activity, oxygen-containing groups, a large surface area, a tunable band gap, excellent adsorption sites, efficient intercalation with various compounds, and excellent electron-transporting properties. These properties make GO an effective adsorbent with good absorptivity and spatial charge separation in hybrid structures formed by arranging monolayers of carbon atoms into a honeycomb structure [8]. Its distinctive structure and electronic properties provide π-π interactions and electrostatic forces, contributing to its high adsorption capacity. GO surfaces are negatively charged and hydrophilic due to an abundance of oxygen-containing functionalities, including hydroxyl, carboxyl, and epoxide groups [9]. By modifying the oxygen functionalities, the band gap of GO can be adjusted, with partially oxidized GO behaving as a semiconductor and fully oxidized GO serving as an electrical insulator. This tunable band gap and electrical conductivity have increased the use of reduced graphene oxide (rGO) in dye adsorption applications in the recent years [10]. rGO is produced by reducing oxygen-containing groups from GO and is effective for dye adsorption due to its defects in the graphitic domain and surface oxygen groups. rGO interacts with dyes through various mechanisms, including π-π electrostatic interactions, structural conjugation, electrostatic interactions, and hydrophobic associations, enabling the adsorption of a wide range of dyes. Because rGO acts as a semiconductor, is cost-effective, and eco-friendly, it has significant potential for use as a metal-free carbonaceous photocatalyst for environmental remediation [11]. Photocatalytic methods offer several advantages compared to other processes. For example, there is no need for the secondary disposal of photocatalysts, and the photocatalytic process is considered eco-friendly as it often occurs at ambient temperature and pressure. Yet, it has some disadvantages like dependency on the light source and the reaction kinetics of photodegradation can be slow, requiring longer treatment times for complete degradation [12]. Therefore, the integrated application of adsorption and photocatalysis can overcome the limitations of each method and provide a more effective and sustainable solution for wastewater treatment.

In this study, GO was synthesized from graphite powder using an improved version of the Hummers' method, which enhances the oxidation process by increasing the amount of $KMnO_4$, instead of using $NaNO_3$, and conducting the reaction in a 9:1 mixture of H_2SO_4 and H_3PO_4. This improved method results in a higher percentage of hydrophilic oxidized graphite material and higher yield compared to Hummers' method [13,14]. Certainly, apart from the Hummers' method, there are alternative techniques for oxidizing the graphite, such as ultrasonic-exfoliation. This method has shown potential in yielding high-quality GO, particularly when paired with compatible surfactants [15]. The exfoliation process under ultrasound can result in GO sheets with a superior aspect ratio and improved colloidal stability, offering advantages for diverse applications [16]. However, it's worth noting that the initial investment for equipment in ultrasound exfoliation tends to be higher compared to the Hummers' method. Nevertheless, this approach often yields GO with fewer defects and enhanced dispersibility compared to direct oxidation methods [15]. The rGO was obtained by thermally reducing GO under vacuum conditions at temperatures of 125, 150, 175, and 200 °C. The thermal reduction provides better control over the degree of reduction and reproducibility [17]. The adsorption capacity and photocatalytic activity of GO and rGO for methylene blue dye were examined, and the role of oxygen functionalities in dye adsorption was assessed. The effect of different experimental conditions such as initial pH, the concentration of dye, the amount of adsorbent and reusability was studied on the adsorption and degradation process.

2. Experimental

2.1. Materials and methods

Synthetic graphite powder with a particle size less than 50 μm, sulfuric acid (H_2SO_4, 97 %), potassium permanganate ($KMnO_4$, 99.5 %), phosphoric acid (H_3PO_4, 88 %), hydrochloric acid (HCl), hydrogen peroxide (H_2O_2, 30 %), and Methylene blue dye (MB) were all of analytical grade. All reactions were conducted using deionized water (DI water with a resistance of approximately 10^7 Ω−cm).

2.2. Characterizations

The crystalline phases of GO and rGO were investigated using X-ray diffraction (XRD) with a PANalytical X-ray Diffractometer, utilizing Cu Kα radiation (wavelength 1.54060 Å) in the 2θ range of 5–70 under 40 mA/45 kV. The functional groups in GO and rGO were analyzed using an FTIR spectrometer (PerkinElmer FTIR). The crystalline structures of GO and rGO were determined by STR 500 COFOCAL MICRO Raman spectroscopy. UV–Vis spectroscopy measurements were conducted with a spectrophotometer (Agilent Carry 5000). Field emission scanning electron microscopy (JEOL JSM 7610 F PLUS) was employed to analyze the surface morphology. Adsorption and photocatalytic activity were assessed using the model dye MB. The Brunauer-Emmett-Teller (BET) study was performed with an Autosorb iQ Station 2 instrument (Quanta chrome instrument) to determine the specific surface area and pores distribution. The photodegradation of MB dye was analyzed by WATERS XEVO G2S QTOF liquid chromatography-mass spectroscopy (LCMS).

2.3. Synthesis of GO and rGO nano-powder

Graphene oxide (GO) was synthesized using an improved version of the Hummers' method for the adsorption and degradation processes [13,14,18]. Initially, 1 gm of graphite powder was combined with a mixture of 120 ml of cool concentrated H_2SO_4 and 15 ml of H_3PO_4, resulting in a black-colored mixture. The stirring was continuously vigorous while maintaining a temperature below 5 °C using an ice bath. Gradually, 6 gm of $KMnO_4$ were added to the mixture below 5 °C and stirred for an additional 30 min. Subsequently, the ice bath was removed, and the mixture was heated to 35 °C for 12 h with continuous stirring. After cooling to room temperature, 120 ml of deionized water (DI water) was introduced to initiate oxidation, ensuring the temperature remained below 60 °C, resulting in a dark brown coloration of the mixture. To terminate the oxidation process, 3 ml of H_2O_2 was slowly added at a temperature of 45 °C, followed by cessation of stirring after 10 min. The mixture underwent filtration and washing with HCl: water (1:10) and subsequently with DI water multiple times until reaching a pH of approximately 7. The resulting precipitate was air-dried at room temperature for 5–6 days and subsequently ground into GO powder.

To prepare rGO, the obtained GO powder was thermally reduced in a vacuum (~10^{-5} Torr) at various temperatures (125, 150, 175, and 200 °C) for 30 min. These samples were labeled as rGO-*x*, where '*x*' represents the reduction temperature.

2.4. Adsorption and photocatalytic process

Adsorption and photocatalytic experiments were conducted using 50 ml of MB dye solution with an initial concentration of 50 ppm. Then, 10 mg of GO/rGO was added to this 50 ml dye solution while vigorously and continuously stirring in the dark. To examine adsorption, 5 ml of the uniformly mixed sample solution was taken out at set time intervals and centrifuged for 2 min at 6000 rpm. After the investigation, it was promptly reintroduced into the main solution along with the centrifuged suspension.

To evaluate photocatalytic activity, the sample solution was illuminated with visible light from a 100-W tungsten lamp (PHILIPS), positioned 15 cm away to cover a 35 cm^2 area of the sample. This exposure commenced after reaching adsorption equilibrium, which typically occurred after 4 h. Continuous stirring was maintained using a magnetic stirrer throughout the process. Likewise, 5 ml of the solution was collected at set time intervals for analysis of photocatalytic activity, then promptly reintroduced into the main solution.

The removal of the dye through adsorption and photocatalytic activities of GO/rGOs were analyzed by UV–Vis spectroscopy, focusing on the characteristic peak of the MB dye observed at a wavelength of 664 nm. Thereafter, the adsorption (C_{ads}), photodegradation (C_{deg}) efficiency and equilibrium adsorption capacity (q_e) of MB dye were calculated accordingly using equations (1)–(3), respectively.

$$C_{ads} = \frac{A_{inital} - A_0}{A_{\text{initial}}} \times 100 = \frac{C_{initial} - C_0}{C_{\text{initial}}} \times 100 \tag{1}$$

$$C_{deg} = \frac{A_0 - A_t}{A_0} \times 100 = \frac{C_0 - C_t}{C_0} \times 100 \tag{2}$$

$$q_e = \left(\frac{C_o - C_e}{m}\right) \times V \tag{3}$$

Here, $C_{initial}$, C_0, C_t and A_{inital}, A_0, A_t are the concentrations (mg/L) and absorbance of MB dye at the initial time, after reaching adsorption-desorption equilibrium, and at the time '*t*', *V* is the volume of the MB solution (L) and *m* is the adsorbent (GO/rGO) dosage in grams [19,20].

3. Results and discussion

(a) Micro-structural analysis

The X-ray diffraction (XRD) spectra of GO and rGO are shown in Fig. 1. In pristine GO an intense (001) diffraction peak was observed at $2\theta = 9.136^{\circ}$ with an interplanar spacing of 0.967 nm, which indicated that the graphite was fully oxidized into GO. After reduction at different temperatures, the (001) peak shifted to a higher 2θ value of 12.455° in rGO-125, and 12.545° in rGO−150 with a decrease in interplanar spacing to 0.705 nm in rGO−150. This is attributed to the removal of some oxygen-containing groups and the decrement of active surface area [21]. The persistence of the (002) peak in both rGO−125 and rGO−150, albeit with diminished intensity, may be attributed to an insufficient reduction temperature. Notably, an increase in reduction leads to a broadening of the peak, as evidenced by the full width at half maximum (FWHM) expanding from 0.59° in the pristine sample to 0.94° in rGO−150. This broadening implies a shift from a larger flake structure to a more granular morphology in samples subjected to higher degrees of reduction [11]. The sample reduced at 175 °C displays a widened peak at approximately 23.136°, accompanied by a minor shoulder peak near 14.038°. The broader (002) peak at 23° signifies well-organized graphite-structured layers, whereas persisting (001) peak around 14° suggests a diminishing presence of oxidized layers of sp^2 hybridized carbon layers [22]. Meanwhile, no prominent peak is evident in the sample reduced at 200 °C, indicative of the prevalence of an amorphous graphite carbon matrix. Furthermore, the presence of the (100) peak around $2\theta = 42.349°$ is notable in rGO−125, rGO−150, and rGO−175, reflecting the turbostratic band of disordered carbon materials [23]. The XRD analysis of the synthesized samples revealed distinct peaks, as indicated in Table 1.

Raman spectroscopy (Fig. 2a-e) is a highly effective tool for the investigation of defects and disorders in crystal structures. All five samples exhibited both the D band and G band of GO [23]. The disorder-induced D band and the Raman-allowed G band are characterized by their intensity ratio, known as the disorder index (I_D/I_G). The D band represents the breathing mode of sp^2 carbon atoms within a hexagonal structure and arises from the formation of structural defects induced by oxygen moieties. Conversely, the G band is associated with the vibration of sp^2 carbon atoms in aromatic rings and is common to all sp^2 carbon forms, resulting from C–C bond stretching [24]. The I_D/I_G ratio, calculated by dividing the maximum peak heights obtained from curve fitting, exhibited a slight decrease from 0.94 in the pristine samples to values of 0.88, 0.86, 0.80, and 0.76 as the reduction temperature increased to 125, 150, 175, and 200 °C, respectively. This decrease in the ratio indicates the removal of most oxygen-containing functionalities, resulting in an increment in the size of sp^2 carbon domains [25]. Additionally, a less prominent band at around 2700 cm^{-1} was observed in the Raman spectra. It may be a possible source of information regarding the number of layers in GO sheets [26].

Fig. 3 displays the FTIR spectra of both graphene oxide (GO) and reduced graphene oxide (rGO). FTIR spectroscopy was utilized to verify the formation of GO and rGO. It identified characteristic peaks corresponding to oxygen-containing groups such as epoxy, carbonyl, and hydroxyl in GO, and confirmed the removal of these oxygen functional groups during the thermal reduction process to form rGO. In the FTIR spectra of GO, an absorption band is observed at 3395 cm^{-1}, corresponding to the stretching vibration of the hydroxyl (–OH) group. This peak, while somewhat flattened, is not completely eliminated in all rGO samples, indicating a partial removal of hydroxyl groups. Additionally, the peak at 1721 cm^{-1}, attributed to C═O stretching, also becomes flattened in all rGO samples due to the partial removal of carbonyl groups [27].

Furthermore, the FTIR spectra of GO exhibit peaks at 1628, 1372, 1223, and 1060 cm^{-1}, corresponding to various oxygen functionalities, namely, aromatic C═C, –O–H bending, epoxy –C–OH stretching, and alkoxy –C–O stretching vibrations, respectively [28].

These FTIR peaks are revealed in Table 2. Notably, the peak at 1628 cm^{-1}, associated with the sp^2 structure of carbon atoms, is also present in all rGO samples, indicating the retention of this structural feature. Moreover, the intensity of peaks at 3395, 1721, and 1372 cm^{-1} in GO decreases significantly upon reduction, underscoring the removal of oxygen-containing functional groups to a certain extent during the reduction process [29].

The surface morphology of both graphene oxide (GO) and reduced graphene oxide (rGO) was analyzed using a field-emission

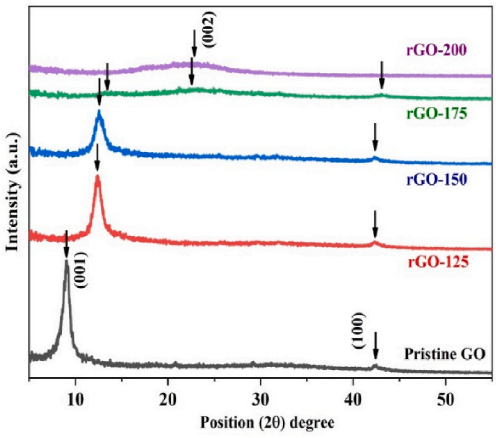

Fig. 1. XRD pattern of GO, rGO−125, rGO−150, rGO−175 and rGO−200.

Table 1
Observed XRD data for synthesized GO and rGOs.

Sample	Peak	Pos.[°2θ]	FWHM [°2θ]	d-spacing [A°]	Rel. Int. [%]
GO	(001)	9.136	1.181	9.679	100.00
	(100)	42.349	0.708	2.134	3.63
rGO−125	(001)	12.455	1.189	7.105	100.00
	(100)	42.357	0.945	2.134	8.06
rGO−150	(001)	12.545	1.417	7.052	100.00
	(100)	42.325	0.708	2.135	10.69
rGO−175	(001)	12.824	4.543	6.897	26.54
	(002)	23.136	10.122	3.841	100.00
	(100)	43.202	2.361	2.092	36.78
rGO−200	(002)	24.215	11.242	3.673	100.00

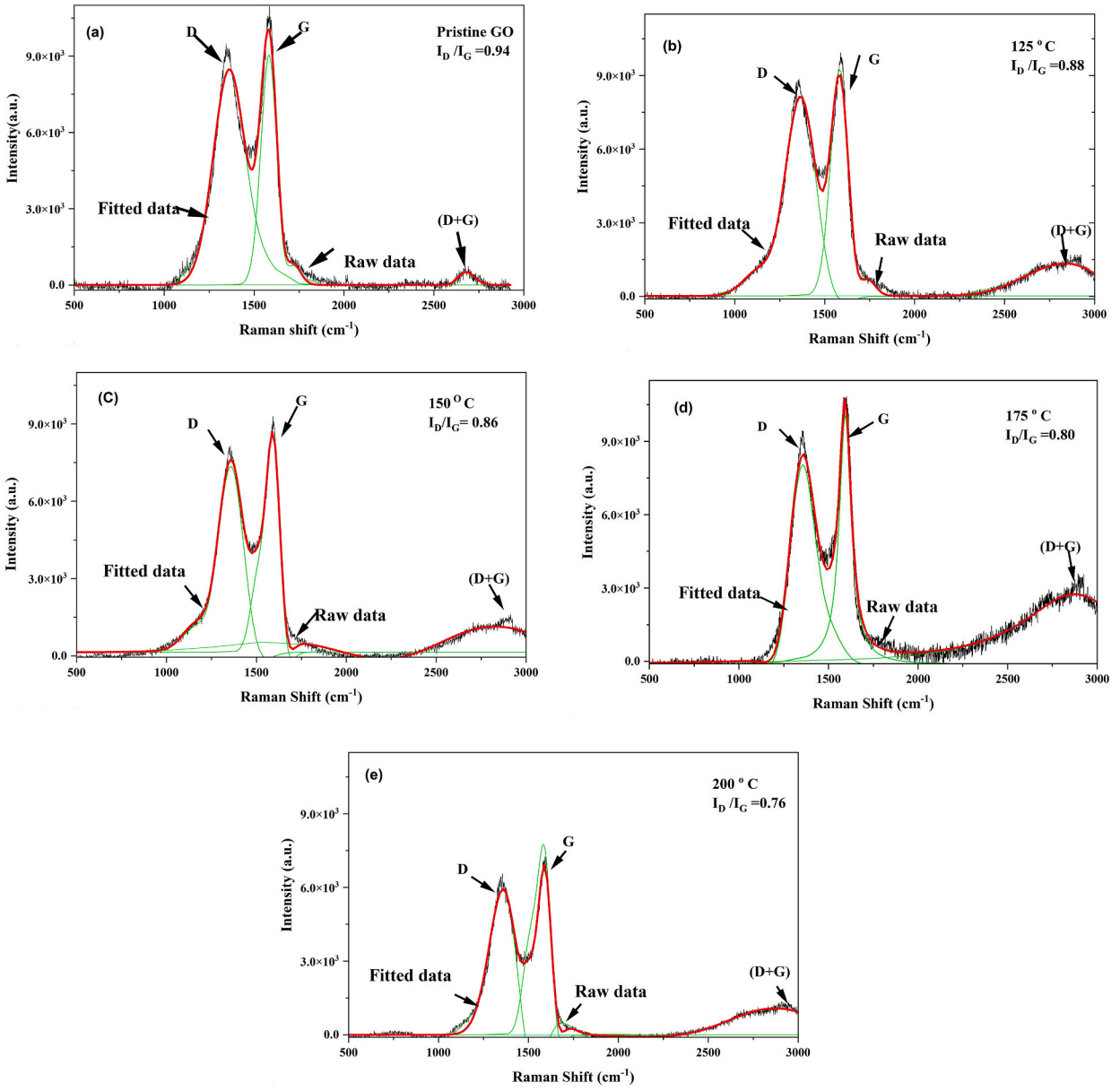

Fig. 2. Raman spectra of (a) GO, (b) rGO−125, (c) rGO−150, (d) rGO−175, and (e) rGO−200.

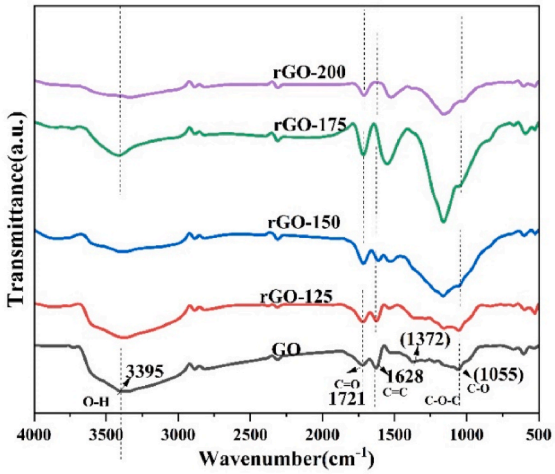

Fig. 3. FTIR spectra of GO, rGO−125, rGO−150, rGO−175, and rGO−200.

Table 2
FTIR data for GO.

S. No.	Wavenumber (cm^{-1})	Bonding
1.	3395	Stretching vibration of the hydroxyl (–OH) group
2.	1721	C═O stretching
3.	1628	Aromatic C═C
4.	1372	–O–H bending
5.	1223	Epoxy –C–OH stretching
6.	1060	Alkoxy –C–O stretching vibrations

scanning electron microscope (FESEM), and the corresponding images are presented in Fig. 4a-e. In the FESEM image of GO, a distinct sheet-like and fluffy microstructure is clearly evident. However, in all rGO samples, the carbon layers of GO undergo exfoliation and appear more clustered, which can be attributed to the thermal reduction process. The FESEM images reveal a notably wrinkled structure in rGO when compared to GO. The absence of charging effects during SEM imaging suggests the electrically conductive behaviour of both GO and rGO, which is linked to their electron charge transport properties [30]. As the degree of reduction increases,

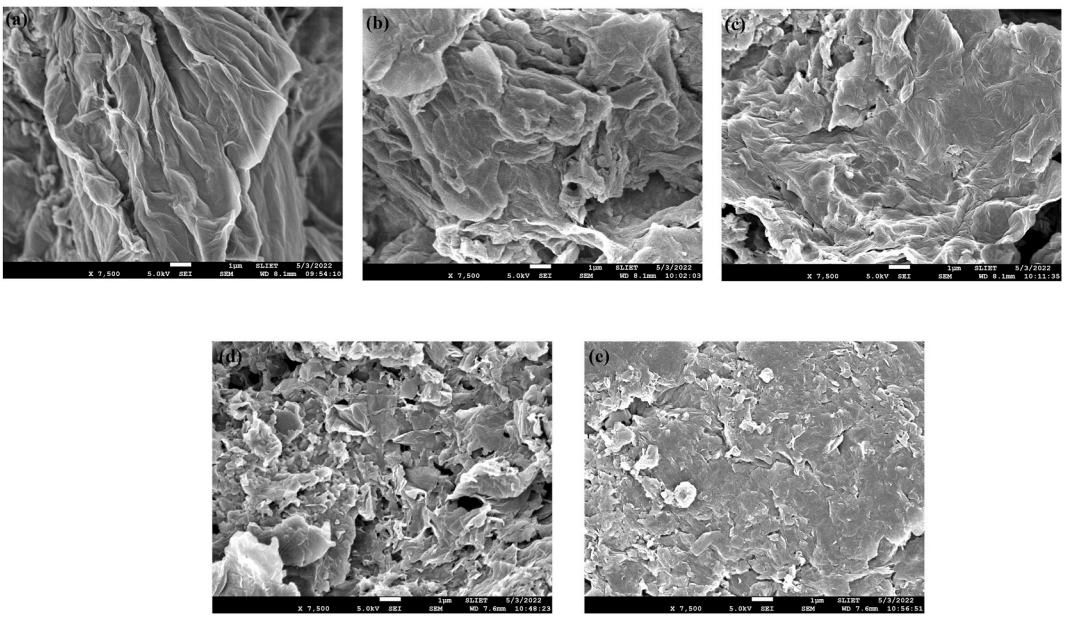

Fig. 4. FESEM image of (a) GO, (b) rGO-125, (c) rGO-150, (d) rGO-175, and (e) rGO-200.

an increased occurrence of cracks on the GO flakes is observed. This suggests a transformation towards a granular microstructure rather than the presence of larger flakes.

The specific surface area and pore volume of the GO and rGO-150 samples were examined using N_2 adsorption–desorption measurement. The corresponding isotherms are depicted in Fig. 5a which is a type IV isotherm that possesses a H3-type hysteresis loop by the IUPAC classification. This indicates the existence of mesopores and the higher volume of gas adsorbed at greater P/P_0 further corroborates the existence of mesopores [20]. The distribution of pore sizes is also illustrated in Fig. 5b. Surface area and pore volume of both GO and rGO-150 was calculated by the BET and BJH method. Our findings indicate that the surface area of rGO-150 is 7.86 m^2/g, which is higher than that of GO (6.610 m^2/g). Additionally, the pore volume was also enhanced from 0.118 cc/g to 0.128 cc/g after reduction [31,32]. However, the BET surface areas of both samples are much lower than the theoretical limit of graphene, which is 2630 m^2/g. The observed discrepancy in BET values can be attributed to the incomplete exfoliation of GO and the coalescence process during thermal reduction [33].

(b) Optical properties of GO and rGO

The UV–Vis absorption spectra observed in the reflectance mode of GO and rGO are shown The UV–Vis absorption spectra observed in the reflectance mode of GO and rGO are shown in Fig. 6a. GO exhibits a characteristic absorption peak at 234 nm corresponding to π-π* transition of the C═C bond of the aromatic ring. This red shift from 234 nm (GO) to 260 nm in rGO-200 may be due to the restoration of sp^2 conjugation and increment of electron concentration in the GO during reduction [34,35]. Another shoulder peak at 309 nm in the pristine GO is due to the n-π* transition of carbonyl group C═O, which disappeared upon the reduction process further confirming the oxygen reduction process [34]. The optical band gap of GO and rGO nanoparticles is deduced from the UV–Vis diffuse reflectance spectra where the Kubelka-Munk function (F(R)) was used and defined as shown in equation (4).

$$F(R) = \frac{(1-R)^2}{2R} = \frac{\alpha}{S} \tag{4}$$

where, 'R' is % reflectance, α is the absorption coefficient and S is the scattering coefficient. The band gap is determined corresponding to indirect transitions according to Tauc' relations (equation (5))

$$(F(R)h\upsilon)^{1/2} = C(E - E_g) \tag{5}$$

where, 'C' is a proportionality constant, 'E_g' is band gap, and 'E' is photon energy. The measured band gap for GO is 2.31 eV, which decreases with the reduction temperature. The band gap is calculated around 1.94, 1.53, 1.12 and 0.73 eV for the samples rGO-125, 150, 175, and 200 °C, respectively indicated in Fig. 6b.

The equilibrium of dye adsorption-desorption on the catalysts/adsorbents was reached after 4 h upon stirring in the dark. The self-degradation of MB in the absence or presence of light is negligible without any catalyst.

Time-dependent C/C_0 plots displaying the adsorption of MB dye by the synthesized GO and rGO samples are shown in Fig. 7. GO exhibits a fast adsorption rate reaching equilibrium even within 30 min. The higher rate of adsorption of MB on GO is due to surface chemistry. The adsorption mechanism can be attributed to electrostatic attraction as it decreases with reduction. Since MB is a cationic dye and graphene oxide surface is highly electronegative because it has a variety of oxygen-containing functional groups at its surface, MB will tend to attach at the surface of GO [36–38]. As the GO is reduced at higher temperatures, the functional groups were removed partially, resulting in attenuation in the rate of adsorption which can be observed from the adsorption rate as mentioned in Table 3. The adsorption rate of MB is calculated by C/C_0, where 'C' is the concentration of MB remaining in the solution after time 't' and 'C_0' is the initial concentration of the standard MB solution. The calculated dye adsorption on GO was 85.78 % in 15 min and 72.35 % in

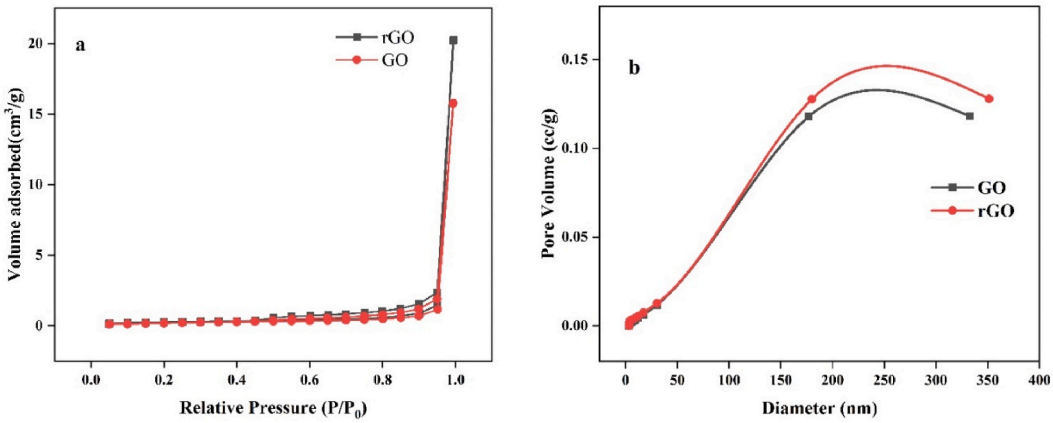

Fig. 5. (a) Nitrogen adsorption–desorption isotherms and (b) BJH pore size distribution curve of GO and rGO−150.

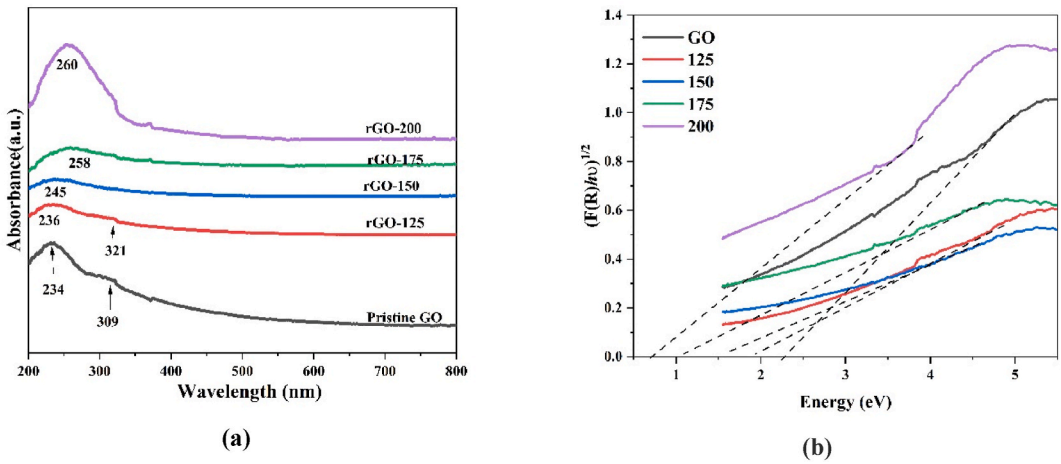

Fig. 6. (a) UV–Vis diffuse spectra of GO, rGO−125, rGO−150, rGO−175, and rGO−200 and (b) Tauc plot for GO, rGO−125, rGO−150, rGO−175, and rGO−200.

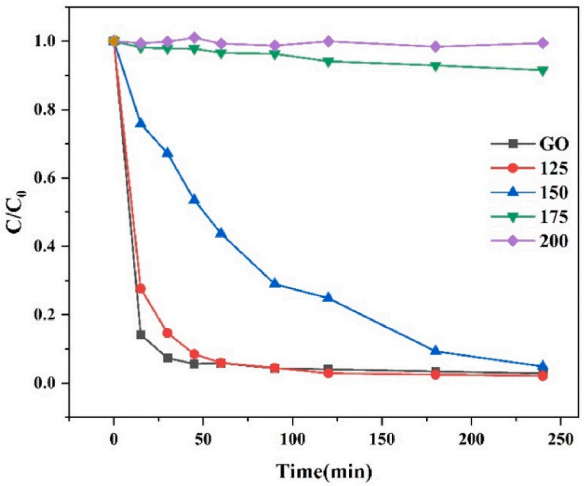

Fig. 7. Time-dependent C/C_0 plots displaying the adsorption of MB dye. (c) MB dye adsorption and photodegradation measurement.

Table 3
Adsorption rate of MB dye and Calculated equilibrium adsorption capacity (q_e) of GO/rGOs.

Time (min) ↓	Adsorption (%)				
	GO	rGO-125	rGO-150	rGO-175	rGO-200
15	85.78	72.35	24.19	1.86	1.01
30	92.68	85.35	32.77	2.12	1.05
45	94.39	91.54	46.46	2.20	1.18
60	94.50	94.06	56.29	3.42	1.58
90	95.64	95.53	71.01	3.71	1.62
120	95.95	97.14	75.17	5.89	1.74
180	96.60	97.51	90.71	7.07	2.31
240	97.18	97.93	95.13	8.51	2.61
q_e (mg/g) →	243.02	247.12	244.50	21.7	6.65

rGO−125. Furthermore, in Table 3 calculated adsorption capacity (q_e) is displayed. The sample rGO−125 exhibited the highest adsorption capacity at 247.12 mg/g, while the sample rGO-150 closely followed with an adsorption capacity of approximately 244.5 mg/g. The adsorption capacity of the sample is notably higher compared to the values 196.8 mg/g and 121.9 mg/g reported for rGO and GO by Bu et al. [39] and Arias et al. [40], respectively. It is noted that GO/rGO, a carbon-based and environmentally friendly metal-free material, exhibits a significant adsorption capacity for removing water pollutants such as dyes. Moreover, a comparative table with additional reported observations is provided in the supplementary material (Figs. S1–S4 and Table S1) for further reference.

Fig. 8 depicts the dye degradation under visible light exposure, with the initial concentration assessed following a 4-h adsorption-desorption equilibrium. As outlined in the preceding section, the adsorption of dye is around 97.18 %, 97.93 %, 95.13 %, 8.51 %, and 2.61 % for GO, rGO−125, rGO−150, rGO−175, and rGO−200. The subsequent reduction was explored via the photocatalytic process, involving the irradiation of the solution with 100−watt visible light to evaluate the photocatalytic activity of the synthesized GO and rGO samples. The higher energy content of the irradiated visible light, emanating from a tungsten lamp, exceeds the catalyst's band gap, leading to the generation of electron-hole pairs and, consequently, the production of reactive oxygen species (ROS), including OH° and O^{2-} to break down the dye molecules. Similar to adsorption, the photocatalytic degradation rate also exhibits an exponential decrease with time (Fig. 8). Notably, GO displays a 30 % degradation, whereas rGO−125 demonstrates a higher degradation of approximately 38 % of the residual dye following adsorption through the photocatalytic process after 3 h of visible light exposure, as specified in Table 4. These results suggest that the higher degradation rate for rGO−150 may be attributed to a narrowed band gap, resulting in a more substantial generation of charge carriers. Consequently, this catalyst achieved an impressive approximately 48 % dye degradation within the same period of 3 h. In contrast, rGO−175 demonstrated lower adsorption and photocatalytic degradation activity compared to rGO−150, potentially attributable to a reduced functional group for the reaction. It is proposed that when dye molecules are adsorbed on the catalyst/adsorbent surface, they may interact more effectively with the ROS compared to when they are freely dispersed in the aqueous solution [11]. Lastly, rGO-200 exhibited minimal degradation of the dye, likely due to the dominance of the amorphous carbon graphite matrix at such an advanced degree of reduction, resulting in an insufficient generation of charge carriers.

Certainly, rGO−150 demonstrates superior performance, manifesting 48 % degradation by the photocatalytic process when compared to its counterparts. However, after the initial dye removal via the adsorption process, further degradation occurs during the subsequent photocatalytic phase. Consequently, the total pollutant removal rates achieved by the different synthesized samples (GO, rGO−125, rGO−150, and rGO−200) over a 7-h period, including 4 h of adsorption-deposition equilibrium followed by 3 h of photocatalytic processing, were recorded as 98.1 %, 98.7 %, 97.4 %, 22.8 %, and 3.7 %, respectively. The heightened photocatalytic activity and superior degradation rate exhibited by rGO−150 may be attributed to its semiconducting properties, which offer the potential for further optimization.

(d) Photocatalytic degradation pathway

The identification of the intermediate and degradation pathways was investigated by liquid chromatography coupled with mass spectrometry (LC−MS) for rGO−150 (spectrograph is provided as Fig. S3 in the supplementary file). The result reveals that the dye degradation is initiated by the demethylation of the molecules [41]. The identified *m/z* (mass-to-charge ratio) values at 301, 284, 271, 256, 242, 230, 218, 158, and 94 in comparison to the peak of MB dye at 284 [41,42] are indicative of potential fragments arising from MB degradation. Additionally, the photocatalytic reaction resulted in the production of intermediate compounds due to the disintegration of benzene rings. Finally, the breakdown of aromatic rings occurs and the resultant smaller intermediates subsequently undergo successive degradation reactions to yield carbon dioxide and water [41,42]. The possible photocatalytic degradation pathway of MB was determined through this study and shown in the supplementary file.

(e) Factors affecting the adsorption and photocatalytic activity

(e−i) Effect of catalyst dose amount: The photocatalytic and adsorption performance of rGO−150 in degrading MB dye was investigated by varying the initial quantities of rGO from 5–20 mg per 50 ml of a 50 ppm MB solution at pH 7. Fig. 9 presents time-dependent C/C_0 plots illustrating the degradation of MB dye at different initial rGO−150 concentrations, while the initial dye concentration (50 ppm) remained constant. The calculated dye adsorption was 20.56, 74.47, 86.22 and 98.48 % for catalyst doses of 5, 10, 15, and 20 mg respectively in 2 h. The results revealed that the removal efficiency of the dye improved with an increase in the quantity of catalyst. This enhancement can be attributed to the greater availability of adsorption sites and an increased surface area for a consistent initial dye concentration. With the augmentation of the catalyst amount, the overall surface area of the photocatalyst expanded, resulting in a higher number of potential adsorption sites [43]. This, in turn, enhanced the dye adsorption process. Additionally, the increased quantity of catalyst particles led to improved photon absorption, facilitating electron and hole generation. Furthermore, it accelerated the rate of reactive oxygen species (ROS) production, which plays a vital role in degrading dye molecules [11].

(e−ii) Effect of initial PH: The adsorption and photocatalytic performance of the catalyst are significantly influenced by the solution's pH. The influence of solution pH on the catalytic activity of the rGO−150 catalyst for MB dye degradation is demonstrated by the C/C_0 graphs in Fig. 10. The dye solution's pH was adjusted between 4 and 11. Throughout the laboratory experiments, the catalyst loading (10 mg) remained constant for 50 ml of MB dye solution with an initial concentration of 50 ppm. The calculated dye adsorption was 24.32, 74.44, 87.99, and 97.74 % for the pH 4, 7, 10, and 12, respectively, in 2 hours. The results indicate that the adsorption efficiency of MB dye is lower in acidic conditions, specifically at pH values lower than neutral. In contrast, when the pH is shifted from

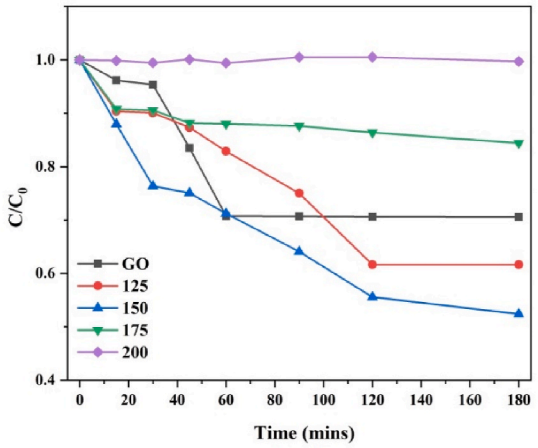

Fig. 8. Time-dependent C/C_0 plots displaying the photocatalytic degradation of MB dye.

Table 4
Degradation through the photocatalytic of the residual MB dye following the adsorption process.

Time (min)	Photocatalytic Degradation (%)				
	GO	rGO-125	rGO-150	rGO-175	rGO-200
15	3.80	9.62	12.05	9.20	0.02
30	4.63	9.93	23.61	9.43	0.42
45	16.48	12.65	24.92	11.81	0.51
60	29.25	17.10	28.77	11.97	0.66
90	29.30	24.95	35.90	12.38	0.79
120	29.38	38.35	44.41	13.60	1.06
180	29.39	38.35	47.58	15.57	1.11

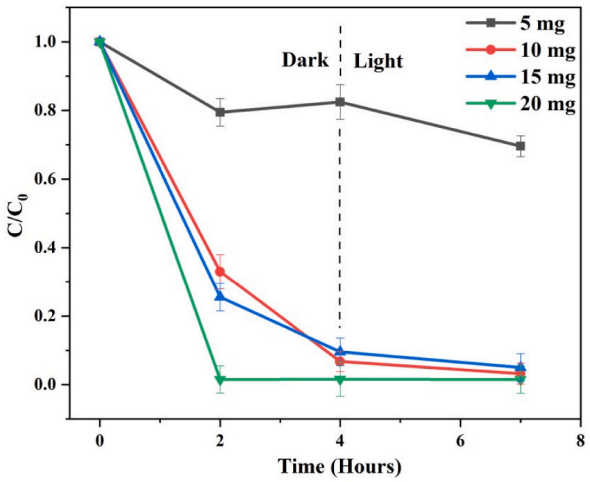

Fig. 9. Time-dependent C/C_0 plots for MB displaying the effect of catalyst dose amount of rGO−150.

neutral to alkaline, the adsorption effectiveness of MB dye experiences a substantial enhancement. In acidic environments, there is an increased presence of hydrogen ions in the solution. This abundance of hydrogen ions leads to increased competition among dye molecules for available adsorption sites on the catalyst's surface. Consequently, the adsorption of dye molecules onto the adsorbent's surface diminishes. Generally, higher pH values prompt GO to adsorb more MB dye. This effect can be attributed to the cationic nature of the dye. At higher pH levels, GO becomes ionized and carries a greater negative charge, which enhances the electrostatic interaction between GO and MB dye [44]. Additionally, the surplus of hydroxyl ions in alkaline conditions promotes the generation of hydroxyl radicals (OH•), further augmenting the photocatalytic degradation rate [45].

(e−iii) Effect of initial dye concentration: The initial dye concentration is a key component that influences the adsorption and

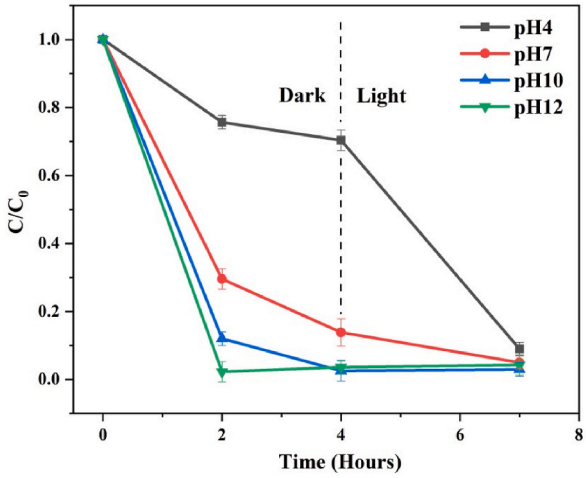

Fig. 10. Time-dependent C/C_0 plots displaying the effect of solution pH for MB over rGO−150.

photodegradation processes [46]. The effect of initial dye concentration on the catalytic activity of the rGO−150 catalyst for MB dye is shown in the C/C_0 plots in Fig. 11. Throughout the laboratory experiments, the catalyst loading (10 mg) and pH (at 7) remained constant, while the dye concentration varied from 30 to 60 ppm. It was observed that the highest dye adsorption occurred at 40 ppm. The calculated dye adsorption was 55.48, 86.22, 74.69, and 50.79 % for the initial dye concentration of 30, 40, 50, and 60 ppm, respectively, in 2 h. The reduced efficiency seen at lower initial dye concentrations could be attributed to less dye adsorbed on the catalyst surface. As a result, the majority of the surface-active sites on the catalyst's surface remain vacant, resulting in the decreased degrading efficiency determined. As the initial concentration of the dye solution increased, more dye molecules were collected on the catalyst surface. This leads to an increase in removal efficiency. At larger dye concentrations, the available adsorption sites eventually became saturated and unable to handle an increasing quantity of dye molecules. The formation of ROS during the photocatalytic dye degradation reaction was also limited due to decreased light photon penetration and a shorter photon path length [19].

(e−iv) Reusability: From the perspective of practical applications, the reusability of a photocatalyst is considered a crucial factor. Photostability and reusability of rGO−150 were investigated by performing four consecutive cycles of adsorption and photocatalytic tests for MB dye, as illustrated in Fig. 12. After each experimental run, the used photocatalyst is collected by centrifugation, washed, and dried at room temperature before being used in the next cycle. The reaction conditions were maintained as similar for each of cycles as are mentioned in the experimental section. The adsorption and photocatalytic performance of rGO−150 are determined to be 97.55, 95.64, 94.06, and 92.67 % for each consecutive cycle, respectively. After four reuse cycles, a slight decrease in the catalyst's photodegradation efficacy is observed. This reduction in photocatalytic activity may be attributed to the loss of photocatalyst during recollection and the deposition of intermediate species on the active sites formed during dye degradation [47].

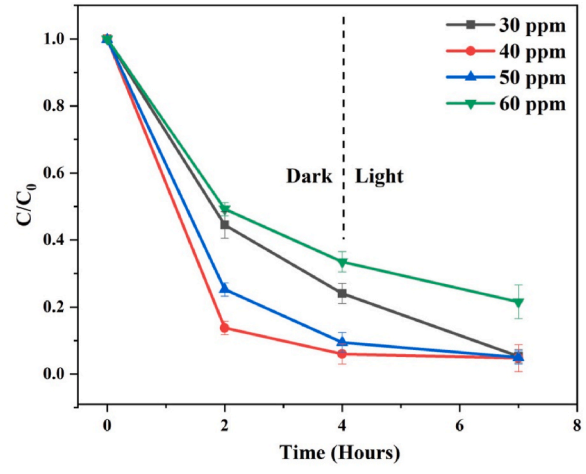

Fig. 11. Time-dependent C/C_0 plots for MB demonstrating the effect of initial dye concentration over rGO−150.

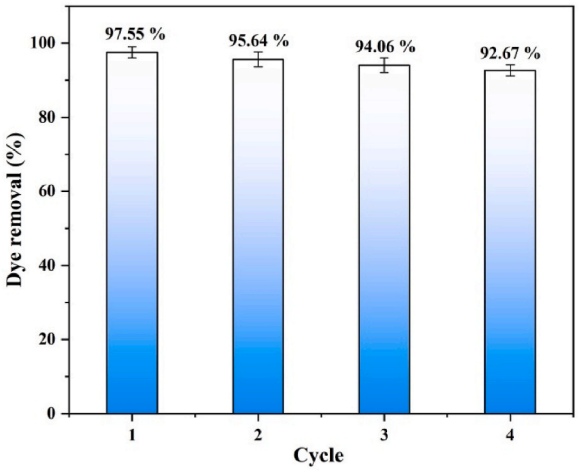

Fig. 12. Reusability tests of rGO−150 for four cycles.

4. Conclusions

GO nanoparticles were synthesized and subjected to thermal reduction at four distinct temperatures (125, 150, 175, and 200 °C) under high vacuum conditions. These nanostructures were assessed for their efficacy in degrading MB dyes through adsorption and subsequent photocatalytic processes. Dye degradation studies revealed that GO serves as a promising adsorbent for removing cationic ions from aqueous solutions. It achieves an impressive 85 % removal of 50 ppm MB dye within just 15 min when utilizing 10 mg of the adsorbent. However, it's important to note that GO itself is not well-suited for photocatalytic degradation. Interestingly, the photocatalytic degradation performance improves after reduction, with the highest degradation rate achieved by rGO−150. Nevertheless, GO reduced at temperatures higher than rGO−150 does not exhibit promising potential for photocatalytic processes. Specifically, GO reduced at 150 °C for 4 h, using 10 mg of sample powder in a 50 ppm MB dye solution, achieves around 95 % removal through the adsorption process. Subsequently, approximately 48 % of the remaining dye can be degraded via the photocatalysis process when exposed to visible light. Overall, these findings suggest that GO, especially when thermally reduced at 150 °C, holds great promise as a carbon-based eco-friendly adsorbent and catalyst for the removal of the cationic dye from aqueous solutions.

Funding

N/A

Ethical approval

The manuscript is not submitted to more than one journal for simultaneous consideration.

Authors have read carefully all the ethics to publish and agree with the terms and conditions of the journal.
The submitted work is original and not have been published elsewhere in any form or language (partially or in full) unless the new work concerns an expansion of previous work.

Consent to participate

N/A

Consent to publish

Authors give their consent to publish the manuscript in this journal after acceptance.

Availability of data and materials

All the data and materials given in the manuscript are generated by the authors and will be provided on request.

CRediT authorship contribution statement

Sanju Mahich: Methodology. **Yogesh Kumar Saini:** Methodology. **Vijay Devra:** Visualization, Validation, Investigation. **Kanika**

Aggarwal: Software, Investigation. **Anuj Kumar:** Visualization, Validation. **Dinesh Kumar:** Writing – review & editing, Supervision. **Amanpal Singh:** Writing – review & editing, Supervision, Conceptualization. **Yogendra Arya:** Writing – review & editing.

Declaration of competing interest

The authors declare that they have no known competing financial interests or personal relationships that could have appeared to influence the work reported in this paper.

Acknowledgements

All authors acknowledge Material Research Centre, MNIT, Jaipur for providing XRD and Raman characterization facilities.

Appendix A. Supplementary data

Supplementary data to this article can be found online at https://doi.org/10.1016/j.heliyon.2024.e31702.

References

[1] P. Singh, P. Shandilya, P. Raizada, A. Sudhaik, A. Rahmani-Sani, A. Hosseini-Bandegharaei, Review on various strategies for enhancing photocatalytic activity of graphene-based nanocomposites for water purification, Arab. J. Chem. 13 (1) (2020) 3498–3520, https://doi.org/10.1016/j.arabjc.2018.12.001.
[2] A.A. Yaqoob, T. Parveen, K. Umar, M.N. Mohamad Ibrahim, Role of nanomaterials in the treatment of wastewater: a Review, Water 12 (2) (2020) 495, https://doi.org/10.3390/w12020495.
[3] S. Thangavel, G. Venugopal, Understanding the adsorption property of graphene-oxide with different degrees of oxidation levels, Powder Technol. 257 (2014) 141–148, https://doi.org/10.1016/j.powtec.2014.02.046.
[4] N. Nagar, V. Devra, Oxidative degradation of Orange G by peroxomonosulfate in presence of biosynthesized copper nanoparticles-a kinetic study, Environ. Technol. Innovat. 10 (2018) 281–289, https://doi.org/10.1016/j.eti.2018.03.005.
[5] G. Kumar, R.K. Dutta, Sunlight-induced enhanced photocatalytic reduction of chromium (VI) and photocatalytic degradation of methylene blue dye and ciprofloxacin antibiotic by Sn_3O_4/SnS_2 nanocomposite, Environ. Sci. Pollut. Res. 29 (38) (2022) 57758–57772, https://doi.org/10.1007/s11356-022-19853-0.
[6] S. De Gisi, G. Lofrano, M. Grassi, M. Notarnicola, Characteristics and adsorption capacities of low-cost sorbents for wastewater treatment: a Review, Sustain. Mater. Technol. 9 (2016) 10–40, https://doi.org/10.1016/j.susmat.2016.06.002.
[7] A. Sandoval, C. Hernández-Ventura, T.E. Klimova, Titanate nanotubes for removal of methylene blue dye by combined adsorption and photocatalysis, Fuel 198 (2017) 22–30, https://doi.org/10.1016/j.fuel.2016.11.007.
[8] F. Khan, M.S. Khan, S. Kamal, M. Arshad, S.I. Ahmadd, S.A.A. Nami, Recent advances in graphene oxide and reduced graphene oxide-based nanocomposites for the photodegradation of dyes, J. Mater. Chem. C 8 (2020) 15940–15955, https://doi.org/10.1039/d0tc03684f.
[9] B. Mao, B. Sidhureddy, A.R. Thiruppathi, P.C. Wood, A. Chen, Efficient dye removal and separation based on graphene oxide nanomaterials, New J. Chem. 44 (2020) 4519–4528, https://doi.org/10.1039/c9nj05895h.
[10] M.A. Kausor, D. Chakrabortty, Graphene oxide-based semiconductor photocatalysts for degradation of organic dye in wastewater: a review on fabrication, Performance Enhancement and challenges, Inorg. Chem. Commun. 129 (2021) 108630, https://doi.org/10.1016/j.inoche.2021.108630.
[11] V.L. Siong, K.M. Lee, J.C. Juan, C.W. Lai, X.H. Tai, C.S. Khe, Removal of methylene blue dye by solvothermally reduced graphene oxide: a metal-free adsorption and photodegradation method, RSC Adv. 9 (2019) 37686–37695, https://doi.org/10.1039/c9ra05793e.
[12] A. Ahmadi, M. Hajilou, S. Zavari, A comparative review on adsorption and photocatalytic degradation of classified dyes with metal/non-metal-based modification of graphitic carbon nitride nanocomposites: synthesis, mechanism, and affecting parameters, J. Clean. Prod. 382 (2023) 134967, https://doi.org/10.1016/j.jclepro.2022.134967.
[13] Jr WS. Hummers, R.E. Offeman, Preparation of graphitic oxide, J. Am. Chem. Soc. 80 (6) (1958), https://doi.org/10.1021/ja01539a017, 1339–1339.
[14] D.C. Marcano, D.V. Kosynkin, J.M. Berlin, A. Sinitskii, Z. Sun, A. Slesarev, L.B. Alemany, W. Lu, J.M. Tour, Improved synthesis of graphene oxide, ACS Nano 4 (8) (2010) 4806–4814, https://doi.org/10.1021/nn1006368.
[15] W.-W. Liu, A. Aziz, Review on the effects of electrochemical exfoliation parameters on the yield of graphene oxide, ACS Omega 7 (38) (2022) 33719–33731, https://doi.org/10.1021/acsomega.2c04099.
[16] S. Park, J. Ann, I. Jung, R.D. Piner, S.J. An, X. Li, A. Velamakanni, R.S. Ruoff, Colloidal suspensions of highly reduced graphene oxide in a wide variety of organic solvents, Nano Lett. 9 (4) (2009) 1593–1597, https://doi.org/10.1021/nl803798y.
[17] A.T. Smith, A.M. LaChance, S. Zeng, B. Liu, L. Sun, Synthesis, properties, and applications of graphene oxide/reduced graphene oxide and their nanocomposites, Nano Mater Sci 1 (1) (2019) 31–47, https://doi.org/10.1016/j.nanoms.2019.02.004.
[18] M.S. Sayem, M.A.H. Suvo, I.M. Syed, M.A. Bhuiyan, Effective adsorption and visible light driven enhanced photocatalytic degradation of rhodamine B using ZnO nanoparticles immobilized on graphene oxide nanosheets, Results Phys. 58 (2024) 107471, https://doi.org/10.1016/j.rinp.2024.107471.
[19] P.L. Meena, K. Poswal, A.K. Surela, J.K. Saini, Synthesis of graphitic carbon nitride/zinc oxide (G-C_3N_4/ZnO) hybrid nanostructures and investigation of the effect of ZnO on the photodegradation activity of G-C_3N_4 against the brilliant cresyl blue (BCB) dye under visible light irradiation, Adv. Compos. Hybrid Mater. 6 (2023) 16, https://doi.org/10.1007/s42114-022-00577-1.
[20] B. Mordhiya, R. Sharma, P.L. Meena, P. Meena, C. Selwal, Development of novel adsorbent for removal of organic contaminant from polluted water: kinetic, isotherm and thermodynamic studies, J. Iran. Chem. Soc. (2024) 1–17, https://doi.org/10.1007/s13738-023-02964-x.
[21] Z. Fan, K. Wang, T. Wei, et al., An environmentally friendly and efficient route for the reduction of graphene oxide by aluminium powder, Carbon 48 (2010) 1686–1689, https://doi.org/10.1016/j.carbon.2009.12.063.
[22] T.F. Emiru, D.W. Ayele, Controlled synthesis, characterization and reduction of graphene oxide: a convenient method for large scale production, Egypt J Basic Appl Sci 4 (2017) 74–79, https://doi.org/10.1016/j.ejbas.2016.11.002.
[23] M.S. Nejad, N. Seyedi, H. Sheibani, Fabrication of functionalized two-dimensional graphene oxide and promoted with phosphotungstic acid for reduction of organic dyes in water, Mater. Chem. Phys. 238 (2019), https://doi.org/10.1016/j.matchemphys.2019.121849, 121849-121849.
[24] S. Perumbilavil, P. Sankar, T. Priya Rose, R. Philip, White light Z-scan measurements of ultrafast optical nonlinearity in reduced graphene oxide nanosheets in the 400-700 nm region, Appl. Phys. Lett. 107 (2015) 051104, https://doi.org/10.1063/1.4928124.
[25] V.G. Sreeja, G. Vinitha, R. Reshmi, et al., Effect of reduction time on third-order optical nonlinearity of reduced graphene oxide, Opt. Mater. 66 (2017) 460–468, https://doi.org/10.1016/j.optmat.2017.01.042.
[26] A. Singh, Y.K. Saini, A. Kumar, S. Gautam, D. Kumar, V. Dutta, H. Lee, J. Lee, S.K. Swami, Property Modulation of graphene oxide Incorporated with TiO_2 for dye-Sensitized solar cells, ACS Omega 7 (48) (2022) 44170–44179, https://doi.org/10.1021/acsomega.2c05637.

[27] I. Sengupta, S. Chakraborty, M. Talukdar, et al., Thermal reduction of graphene oxide: how temperature influences purity, J. Mater. Res. 33 (2018) 4113–4122, https://doi.org/10.1557/jmr.2018.338.
[28] D. He, Z. Peng, W. Gong, et al., Mechanism of a green graphene oxide reduction with reusable potassium carbonate, RSC Adv. 5 (2015) 1196611972, https://doi.org/10.1039/c4ra1451a.
[29] C. Xu, X. Shi, A. Ji, et al., Fabrication and characteristics of reduced graphene oxide produced with different green reductants, PLoS One 10 (12) (2015), https://doi.org/10.1371/journal.pone.0144842.
[30] M. Strankowski, Ł. Piszczyk, P. Kosmela, P. Korzeniewski, Morphology and the physical and thermal properties of thermoplastic polyurethane reinforced with thermally reduced graphene oxide, Pol. J. Chem. Technol. 17 (2015) 88–94, https://doi.org/10.1515/pjct-2015-0073.
[31] P. Das, S. Ibrahim, K. Chakraborty, S. Ghosh, T. Pal, Stepwise reduction of graphene oxide and studies on defect-controlled physical properties, Sci. Rep. 14 (1) (2024) 294, https://doi.org/10.1038/s41598-023-51040-0.
[32] D.H. Carrales-Alvarado, I. Rodríguez-Ramos, R. Leyva-Ramos, E. Mendoza-Mendoza, D.E. Villela-Martínez, Effect of surface area and physical–chemical properties of graphite and graphene-based materials on their adsorption capacity towards metronidazole and trimethoprim antibiotics in aqueous solution, Chem. Eng. J. 402 (2020) 126155, https://doi.org/10.1016/j.cej.2020.126155.
[33] B. Zhao, P. Liu, Y. Jiang, D. Pan, H. Tao, J. Song, T. Fang, W. Xu, Supercapacitor performances of thermally reduced graphene oxide, J. Power Sources 198 (2012) 423–427, https://doi.org/10.1016/j.jpowsour.2011.09.074.
[34] F. Zheng, W.-L. Xu, H.-D. Jin, et al., Charge transfer from poly(3-hexylthiophene) to graphene oxide and reduced graphene oxide, RSC Adv. 5 (2015) 89515–89520, https://doi.org/10.1039/c5ra18540h.
[35] C. Wong, C. Lai, K. Lee, S. Hamid, Advanced chemical reduction of reduced graphene oxide and its photocatalytic activity in degrading reactive black 5, Materials 8 (2015) 7118–7128, https://doi.org/10.3390/ma8105363.
[36] P. Ranjan, P. Verma, S. Agrawal, et al., Inducing dye-selectivity in graphene oxide for cationic dye separation applications, Mater. Chem. Phys. 226 (2019) 350–355, https://doi.org/10.1016/j.matchemphys.2019.01.047.
[37] P. Bradder, S.K. Ling, S. Wang, S. Liu, Dye adsorption on layered graphite oxide, J. Chem. Eng. Data 56 (1) (2010) 138–141, https://doi.org/10.1021/je101049g.
[38] N. Jahan, H. Roy, A.H. Reaz, S. Arshi, E. Rahman, S.H. Firoz, M.S. Islam, A comparative study on sorption behavior of graphene oxide and reduced graphene oxide towards methylene blue, Case Studies Chem Environm Eng 6 (2022) 100239, https://doi.org/10.1016/j.cscee.2022.100239.
[39] J. Bu, L. Yuan, N. Zhang, D. Liu, Y. Meng, X. Peng, High-efficiency adsorption of methylene blue dye from wastewater by a thiosemicarbazide functionalized graphene oxide composite, Diam. Relat. Mater. 101 (2020) 107604, https://doi.org/10.1016/j.diamond.2019.107604.
[40] F.A. Arias, M. Guevara, T. Tene, P. Angamarca, R. Molina, A. Valarezo, L.S. Caputi, The adsorption of methylene blue on eco-friendly reduced graphene oxide, Nanomater 4 (2020) 681, https://doi.org/10.3390/nano10040681.
[41] M.A. Rauf, M.A. Meetanib, A. Khaleel, A. Ahmed, Photocatalytic degradation of methylene blue using a mixed catalyst and product analysis by LC/MS, Chem. Eng. J. 157 (2–3) (2010) 373–378, https://doi.org/10.1016/J.CEJ.2009.11.017.
[42] A. Rathore, V. Devra, Azadirachta indica Leaf Mediated Synthesis of iron nanoparticles and their catalytic application in methylene blue degradation, Catalysis Res 3 (1) (2023) 1–12, https://doi.org/10.35702/catalres.10008.
[43] M. Said, M. Ulfa, Addy Rachmat, et al., Synthesis of reduced graphene oxide from cellulose and its applications for methylene blue adsorption, Solid State Phenom. 345 (2023) 153–170, https://doi.org/10.4028/p-n4sufo.
[44] C. M. B.de Assis Filho de Araujo, et al., Systematic study of graphene oxide production using factorial design techniques and its application to the adsorptive removal of methylene blue dye in aqueous medium, Mater. Res. Express 5 (6) (2018) 065042, https://doi.org/10.1088/2053-1591/aacb51.
[45] S.-T. Yang, S. Chen, Y. Chang, A. Cao, Y. Liu, H. Wang, Removal of methylene blue from aqueous solution by graphene oxide, J. Colloid Interface Sci. 359 (2011) 24–29, https://doi.org/10.1016/j.jcis.2011.02.064.
[46] I. Khan, K. Saeed, N. Ali, I. Khan, B. Zhang, M. Sadiq, Heterogeneous photodegradation of industrial dyes: an insight to different mechanisms and rate affecting parameters, J. Environ. Chem. Eng. 8 (5) (2020) 104364, https://doi.org/10.1016/j.jece.2020.104364.
[47] A.G. Sundaram, K. Namasivayam, L. Ramesh, S.P.D. Sadhasivam, Synthesis, characterization, and enhanced sunlight-active photocatalytic property of single-site octahedral iron (III) oxide complex–grafted graphene oxide, J Alloys Compounds 968 (2023) 172068, https://doi.org/10.1016/j.jallcom.2023.172068.